Advantages of Hyperspectral over RGB image on Land Cover Classification

1st Cheng Hao Ko
Graduate Institute of Automation and Control
National Taiwan University of Science and Technology
Taipei, Taiwan
kevin.ko@mail.ntust.edu.tw

2nd Jajang Jaenudin*
Graduate Institute of Automation and Control
National Taiwan University of Science and Technology
Taipei, Taiwan
Mechatronics Department
Politeknik Caltex Riau
Pekanbaru, Indonesia
jajang@pcr.ac.id

3rd Vincentius Christian Bintang
Graduate Institute of Automation and Control
National Taiwan University of Science and Technology
Taipei, Taiwan
bintangvincent@gmail.com

4th Jih-Run Tsai
National Space Organization (NSPO)
Taiwan
Hsinchu, Taiwan
jrtsai@nspo.narl.org.tw

5th Shin Fan Lin
National Space Organization (NSPO)
Taiwan
Hsinchu, Taiwan
sflin@nspo.narl.org.tw

6th Jiun-Kai Tseng
Graduate Institute of Automation and Control
National Taiwan University of Science and Technology
Taipei, Taiwan
tseng.kai@gmail.com

***Abstract*—Crop identification and land cover estimation are essential for farming and land management practices in the precision agriculture field. Conventional measurements are expensive and time-consuming and thus cannot be treated as appropriate for large areas. An automatic crop or land classification should be applied to overcome these problems. Therefore, high-quality data availability is required to feed the classification tools. To fulfill the needs, we have used an airborne system for collecting in the Taiwan agriculture area. A VNIR hyperspectral image has been proven to significantly increasing accuracy compared to an RGB image. With simple discriminant algorithm LD and QD, the classification accuracy of VNIR images reaches 88.14 % and 92.02%, respectively. Meanwhile, RGB images attain 52.73% and 52.27%.**

Keywords—RGB Image, Hyperspectral Image, Separability, Classification, Accuracy.

I. INTRODUCTION

Agriculture is an important socio-economic element that needs to develop to sustain national food security continually. From a business, perspective is essential to know to forecast the supply and demand of the particular farm commodity, plan landscape management, and regulate the market price [1].

Remote sensing is one of the technical methods in precision agriculture mapping to forecast the farm product in industry 4.0 emergence [2]. This technique can tackle ineffective and inefficient traditional ways because the direct field investigation by measuring the farm landscape manually. one way to utilize technological method development to optimize the cost-benefit process in production forecasting. Hence the intelligent agriculture innovation can contribute.

One standard method for automatic crop yield estimation uses airborne remote sensing and classification methods to identify the crop species. The emerging of remote sensing is supported by the technology development of existing imaging sensors. The hyperspectral imaging (HSI) sensor can offer broader information compare to Multispectral (MS) and RGB sensors [3][4]. As the state-of-the-art data cube with a broader band, HSI can provide richer features that enhance the classification performance [5].

Remote sensing using UAV or satellite [6] as an imaging device platform combined with machine learning methods is standard in object detection and mapping [7]. The technique of taking pictures using an airborne system allows hyperspectral cameras to be transported, which is not yet possible with UAVs. In addition to having a vast spectrum from VNIR to SWIR with a very high resolution (3-10 nm) per band, the resulting image also has a competitive spatial resolution compared to UAV systems. Increasing the number of features will increase class separability, wherein images with limited features between one class and another class with similar characteristics cannot be separated/classified. However, with the addition of feature data, the differences in characteristics between classes become more significant. With the bursting of features in hyperspectral data, of course, it will not be very easy for computation if using complex classification algorithms [8]. Therefore, selecting a simple algorithm such as the discriminant classifier is intended to make the training and testing process more efficient [9]. The

research aims to provide direction on the importance of hyperspectral data in mapping a specific area. Even with a simple algorithm method, the classification performance can achieve a reasonably high performance compared to using only RGB images.

The research aims to provide direction on the importance of hyperspectral data in mapping a particular area. Even with a simple algorithm method, the classification performance can achieve a reasonably high performance compared to using only RGB images. Therefore, in this works, it will be shown that replacing RGB data with hyperspectral data can improve the performance of a structurally simple classifier.

The problem of mapping agricultural land is that it is ineffective and inefficient if the investigation is carried out manually, directly in the field. It takes a long time and a very high cost to map a large area. The use of imaging with aerial photos is beneficial for the land cover classification process. However, imaging consisting only of the RGB spectrum is not reliable enough when classified using a simple classification method. Reliable imaging with more spatial resolution and spectrum is required. The classification accuracy of RGB images may be improved by choosing a more complex algorithm such as SVM [10] or even by deep learning [11]. However, this method will not be effective because the spectral features are minimal. In this work, many methods for getting Non-RGB images with various spatial and spectral resolutions, such as satellite, airborne, or unmanned aerial vehicles (UAV). The platform is used a manned plane that carries the hyperspectral imaging system to do so farmland landscape scanning mission.

The drawback of using hyperspectral data compared to RGB is the redundancy of feature information contained within it [12]. Thus, it is necessary to unmix or reduce the dimensional spectral features to gain better separability. Principal component analysis (PCA) is the standard method to reduce the spectral into its most significant feature is principal component analysis (PCA). This method significantly improves spectral classification by finding the most principle band to differentiate between similar classes. These steps are only crucial for sophisticated methods. This works omit this procedure and include all bands because of the simplicity of discriminant analysis.

Therefore, in this presentation, it will be shown that replacing RGB data with hyperspectral data can improve the performance of a classifier that is structurally very simple.

II. Study Area and Data Set

A. Study Area

The study area is part of Yunlin County (southwest Taiwan), located between 120°20'58"E–120°21'6"E and 23°44'22" N –23°44'29" N (around 59.624 m^2). RGB and VNIR hyperspectral image on study area shown in Fig. 1. Some different crops and soil cover the area.

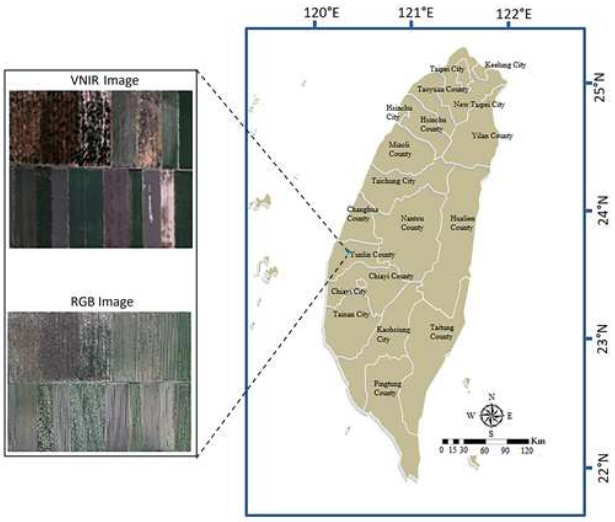

Fig. 1. VNIR and RGB image on the study area

B. Data Set

The UAV system has taken the RGB image. Meanwhile, the hyperspectral is collected by the airborne system. The Taiwan Agriculture Research Institute (TARI) served the ground truth or label by direct field investigation. The label is shown in Fig. 2.

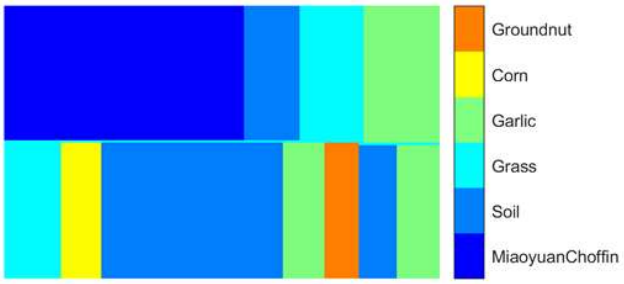

Fig. 2. Label for training and testing data set

The data set spatial size is 331-pixel x 367 pixels, a total of 121.477 pixels consisting of 6 different imbalanced classes. The data has been split 30% for training and 70% for testing. Class pixel distribution is shown in Table I.

TABLE I. Class Pixel Distribution

No.	Class Name	Number of Pixels	Pixel for Training	Pixel for Testing
1	Miaoyuan	33.128	10.100	23.028
2	Soil	38.169	11.600	26.569
3	Grass	17.518	5.100	12.418
4	Garlic	22.267	6.750	15.517
5	Corn	5.610	1.700	3.910
6	Groundnut	4.785	1.450	3.335
Total pixels		121.477	36.700	84.777

III. Data Characteristic

An RGB (red, green, blue) image is a three-dimensional byte array that explicitly stores a color value for each pixel. RGB image arrays are three channels of color information.

Meanwhile, a hyperspectral image consists of hundreds or thousands of narrower bands (10-20 nm). Fig. 3 shows the spectrum of RGB and hyperspectral images. Jeffries-Matisuta value is used to check the separability between classes of both RGB and hyperspectral images.

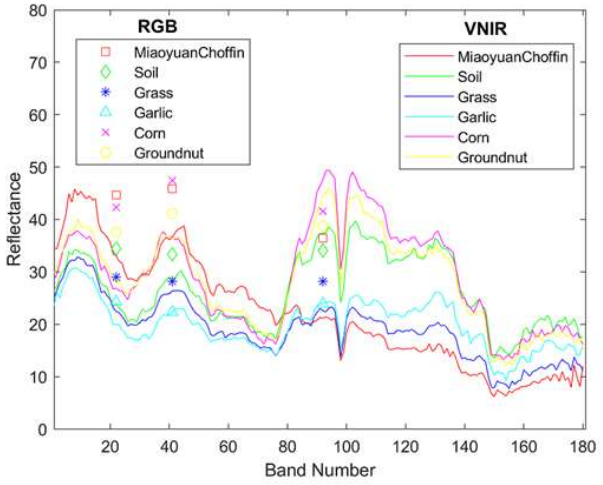

Fig. 3. RGB and VNIR spectral signature

The Jeffries–Matusita (J–M) distance method [13][14] is suitable to describe the class separability of multispectral or hyperspectral images. This method is based on Bhattacharyya distance, one of the most common ways to predetermine the statistical separability of two classes of materials. This distance measure in terms of only the first two moments of these two density functions is

$$B=\frac{1}{8}\left[\mu_x-\mu_y\right]^T\left[\frac{\Sigma_x+\Sigma_y}{2}\right]^{-1}\left[\mu_x-\mu_y\right]+\frac{1}{2}\ln\frac{\left|\frac{1}{2}\left[\Sigma_x+\Sigma_y\right]\right|}{\sqrt{\left|\Sigma_x\right|\left|\Sigma_y\right|}} \quad (1)$$

where $\sum$ is the covariance matrix, $\Sigma=\sigma^2$

Large values of B imply small upper limits on the Bayes error and hence good separability. As a measure of separability, the Bhattacharyya distance has the disadvantage of growing even after the classes have become so well separated that any classification procedure could distinguish them. The Jeffries–Matusita (J-M) distance measures the separability of two classes on a more convenient scale $[0-2]$ in terms of B:

$$J=2\left(1-e^{-B}\right) \quad (2)$$

as B continues to grow, the measure saturates at the value 2. Calculating by estimating the class means and covariance matrices. Table II shows that the RGB image's J-M value is relatively lower than two, which means the RGB separability is sub-optimal. On the other hand, the J-M value of the VNIR image is closest to 2, mean very high separability. These data characteristics will affect the classification accuracy.

TABLE II. J-M DISTANCE OF RGB/VNIR IMAGES

Classes	Miaoyuan Chooffin	Soil	Grass	Garlic	Corn	Ground nut
Miaoyuan Chooffin	0 / 0	0,65 / 2	0,48 / 2	1,05 / 2	0,49 / 2	1,2 / 2
Soil	0,65 / 2	0 / 0	0,24 / 1,99	0,51 / 1,98	0,33 / 2	0,8 / 2
Grass	0,48 / 2	0,24 /	0 / 0	0,52 / 2	0,25 / 2	0,82 / 2
Garlic	1,05 / 2	0,51 /	0,52 / 2	0 / 0	0,34 / 2	1,19 / 2
Corn	0,49 / 2	0,33 / 2	0,25 / 2	0,34 / 2	0 / 0	1,12 / 2
Groundnut	1,2 / 2	0,8 / 2	0,82 / 2	1,19 / 2	1,12 / 2	0 / 0

IV. DISCRIMINANT CLASSIFIER

In this experiment, we use a discriminant classifier because of the simplicity of its algorithm structure—there are two kinds of kernel: linear and quadratic.

A. *Linear Discriminant*

LD is a fast and straightforward statistical method to separate two or multiple classes by fitting the estimation model into the data based on its gaussian distribution. The decision boundaries are placed between the gaussian distribution of different categories as a line[15]. The algorithm also uses the dimensionality reduction method by maximizing the increase in class separability. The sparse feature can make the classification easier due to it being linearly separable[16]. The distribution characteristics can be measure using the covariance and means of all data.

LD can be used as a supervised classification[15], [17] tool for k classes. The key steps assume a rule to divide the scattering data into k number of areas that belong to each observed data. The Maximum likelihood to allocate the data is used:

$$j=\arg\max_i f_i(x) \quad (3)$$

or Bayesian rules

$$j=\arg\max_i \pi_i f_i(x) \quad (4)$$

From the datasets, the discriminant function for all classes for each observation can be written as:

$$\delta_i(x)=\log f_i(x)+\log\pi_i \quad (5)$$

with the assumption that all classes are distributed with the same covariance matrix, the discriminant for the decision boundary can be written as a linear function:

$$\delta_k(x)=x^T\Sigma^{-1}\mu_k-\frac{1}{2}\mu_k^T\Sigma^{-1}\mu_k+\log\pi \quad (6)$$

B. *Quadratic Discriminat*

For the quadratic analysis (QDA), the decision boundary is nonlinear because the quadratic terms remain, so the discriminant function can be rewritten as follow:

$$\delta_k(x) = -\frac{1}{2}\log|\Sigma_k| - \frac{1}{2}(x-\mu_k)^T \Sigma_k^{-1}(x-\mu_k) + \log \pi_k$$

(7)

the quadratic type tends more flexibly than a linear one.

V. RESULT AND DISCUSSION

In this paper, the performance classification indicated by three kinds of accuracy used: Overall Accuracy (OA), Average Accuracy (AA), and Cohen's kappa coefficient (κ), consecutively defined by

$$OA = \frac{1}{N}\sum_{i=1}^{r} n_i$$

(8)

$$AA = \frac{1}{k}\sum_{c=1}^{k} A_c$$

(9)

$$\kappa = \frac{P_o - P_e}{1 - P_e}$$

(10)

where,

$$P_o = OA \text{ and } P_e = \frac{1}{N^2}\sum_k n_{k1} n_{k2}$$

N: Total sample
n_i: Correct prediction of pixel i
r: Total correct prediction
k: Number of classes
A_c: Accuracy of Class c
n_{ki}: Number of items classified as k by rater i

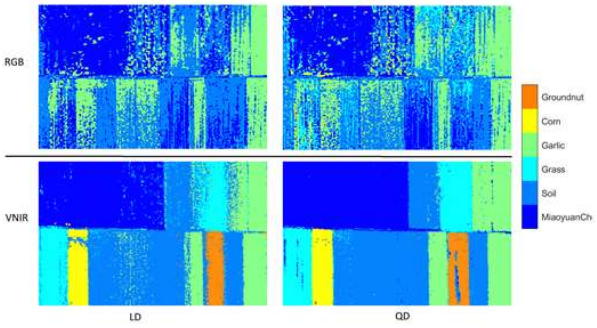

Fig. 4. Map classification results

Classification Mapping is shown in Fig.4. The experimental results show a significantly increased accuracy for both AA, OA, and Kappa on using a 180 band VNIR image compared to a three-band RGB image. As seen in the RGB image, the groundnut and corn classes cannot be detected by the LD at all. Using QD, groundnut is still not detected, and corn has started to be detected by a few pixels. Misclassification occurs in several areas. OA accuracy rate is still shallow at around 50%. The detail of each class's accuracy for each image type with respective methods is shown in Table III.

TABLE III. PER CLASS ACCURACY

Image Type	Classifier	Classes					
		Miaoyuan Choffin	Soil	Grass	Garlic	Corn	Groundnut
RGB	LD	75.88	64.1	0,49	65,3	0	0
	QD	69,16	54,6	27,0	66,3	5,17	0
VNIR	LD	90,32	93,8	79,8	82,7	85,1	87,20
	QD	95,36	97,0	89,4	92,3	94,0	85,58

However, using VNIR image data, simple LD and QD algorithms have detected all existing classes with reasonable accuracy, as shown in Fig.5. With the addition of so many bands, the discrimination function between classes becomes more apparent, increasing the separability, making it easier for the classifier to separate. The level of accuracy is relatively high in the range of numbers, more than 90%.

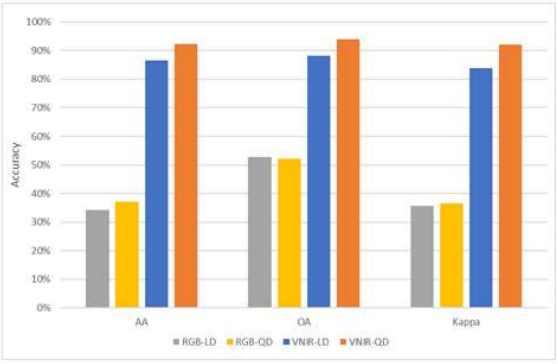

Fig. 5. Performance of RGB vs. VNIR image classification by LD and QD

TABLE IV. METHODS TIME COSTS

Image Type	Classifier	Training Time	Testing Time
RGB	LD	1.64	0.14
	QD	0.77	0.06
VNIR	LD	8.62	2.17
	QD	8.62	2.29

The combination between data type and the methods applied shows in Table IV that discriminant analysis has rapid execution with an average of 8 seconds for training time with a sample size of 36,700 and 2 seconds for testing with a sampling size of 84,777. Even with RGB data is significantly lower than VNIR however, the hyperspectral data time processing is quite acceptable under 10 seconds. Thus it indicates the computation efficiency and rapid performance for classification using discriminant analysis.

VI. CONCLUSION

Hyperspectral VNIR data was very significant in increasing the accuracy of land cover classification compared to RGB images. Abundant features can increase separability between classes. However, high separability does not guarantee high accuracy for classes with a limited number of training samples. The type of kernel/filter selected is also very influential on the classification results. With RGB image, the Quadratic kernel has not increased the accuracy value

compared to the Linear kernel. However, with VNIR data, there was a very significant increase. Meanwhile, training and testing time is still fast. Kernel development in discriminant analysis can further improve classification accuracy while maintaining short training and testing times.

ACKNOWLEDGMENT

The authors would like to acknowledge NSPO Taiwan for their support and funding of this research and TARI for providing ground truth data of our study area.

REFERENCES

[1] S. J. Scherr, S. Shames, and R. Friedman, "From climate-smart agriculture to climate-smart landscapes," pp. 1–15, 2012.

[2] J. Ruan *et al.*, "Agriculture IoT: Emerging Trends, Cooperation Networks, and Outlook," *IEEE Wirel. Commun.*, vol. 26, no. 6, pp. 56–63, 2019, DOI: 10.1109/MWC.001.1900096.

[3] E. Honkavaara *et al.*, "Remote Sensing of 3-D Geometry and Surface Moisture of a Peat Production Area Using Hyperspectral Frame Cameras in Visible to Short-Wave Infrared Spectral Ranges Onboard a Small Unmanned Airborne Vehicle (UAV)," *IEEE Trans. Geosci. Remote Sens.*, vol. 54, no. 9, pp. 5440–5454, 2016, DOI: 10.1109/TGRS.2016.2565471.

[4] P. Singh *et al.*, *Hyperspectral remote sensing in precision agriculture: present status, challenges, and future trends*. LTD, 2020.

[5] P. Ghamisi *et al.*, "Advances in Hyperspectral Image and Signal Processing: A Comprehensive Overview of the State of the Art," *IEEE Geosci. Remote Sens. Mag.*, vol. 5, no. 4, pp. 37–78, 2017, DOI: 10.1109/MGRS.2017.2762087.

[6] Z. Sun, D. Wang, and G. Zhong, "A review of crop classification using satellite-based polarimetric SAR imagery," *2018 7th Int. Conf. Agro-Geoinformatics, Agro-Geoinformatics 2018*, pp. 3–7, 2018, DOI: 10.1109/Agro-Geoinformatics.2018.8476020.

[7] P. Aposporis, "Object Detection Methods for Improving UAV Autonomy and Remote Sensing Applications," *Proc. 2020 IEEE/ACM Int. Conf. Adv. Soc. Networks Anal. Mining, ASONAM 2020*, pp. 845–853, 2020, DOI: 10.1109/ASONAM49781.2020.9381377.

[8] G. Taskin, H. Kaya, and L. Bruzzone, "Feature selection based on high dimensional model representation for hyperspectral images," *IEEE Trans. Image Process.*, vol. 26, no. 6, pp. 2918–2928, 2017, DOI: 10.1109/TIP.2017.2687128.

[9] H. Yuan, Y. Y. Tang, Y. Lu, L. Yang, and H. Luo, "Spectral-spatial classification of hyperspectral image based on discriminant analysis," *IEEE J. Sel. Top. Appl. Earth Obs. Remote Sens.*, vol. 7, no. 6, pp. 2035–2043, 2014, DOI: 10.1109/JSTARS.2013.2290316.

[10] G. Mountrakis, J. Im, and C. Ogole, "Support vector machines in remote sensing: A review," *ISPRS Journal of Photogrammetry and Remote Sensing*, vol. 66, no. 3. pp. 247–259, May 2011, DOI: 10.1016/j.isprsjprs.2010.11.001.

[11] L. Ma, Y. Liu, X. Zhang, Y. Ye, G. Yin, and B. A. Johnson, "Deep learning in remote sensing applications: A meta-analysis and review," *ISPRS J. Photogramm. Remote Sens.*, vol. 152, no. March, pp. 166–177, 2019, DOI: 10.1016/j.isprsjprs.2019.04.015.

[12] S. Sattar, H. Ahmad Khan, and K. Khurshid, "Optimized class-separability in hyperspectral images," *Int. Geosci. Remote Sens. Symp.*, vol. 2016-November, pp. 2711–2714, 2016, DOI: 10.1109/IGARSS.2016.7729700.

[13] M. Dabboor, S. Howell, M. Shokr, and J. Yackel, "The Jeffries–Matusita distance for the case of complex Wishart distribution as a separability criterion for fully polarimetric SAR data," *Int. J. Remote Sens.*, vol. 35, no. 19, pp. 6859–6873, 2014, DOI: 10.1080/01431161.2014.960614.

[14] P. Kumar, R. Prasad, A. Choudhary, V. N. Mishra, D. K. Gupta, and P. K. Srivastava, "A statistical significance of differences in classification accuracy of crop types using different classification algorithms," *Geocarto Int.*, 2017, DOI: 10.1080/10106049.2015.1132483.

[15] B. Ghojogh and M. Crowley, "Linear and Quadratic Discriminant Analysis: Tutorial," *arXiv*, no. 4. pp. 1–16, 2019, [Online]. Available: https://arxiv.org/pdf/1906.02590.pdf.

[16] C. Xia, S. Yang, M. Huang, Q. Zhu, Y. Guo, and J. Qin, "Maize seed classification using hyperspectral image coupled with multi-linear discriminant analysis," *Infrared Phys. Technol.*, vol. 103, no. July, p. 103077, 2019, DOI: 10.1016/j.infrared.2019.103077.

[17] Q. Du and R. Nekovei, "Implementation of real-time constrained linear discriminant analysis to remote sensing image classification," *Pattern Recognit.*, vol. 38, no. 4, pp. 459–471, 2005, DOI: 10.1016/j.patcog.2004.09.008.